Stroke and Its Imaging Evaluation

18

Sathish Kumar Dundamadappa, Melanie Ehinger, and Andrew Chen

Introduction

Stroke, defined as the sudden onset of persistent neurologic deficit, is a significant cause of morbidity and mortality in the USA. It is the third leading cause of death [1]. Ischemic infarction is by far the most common etiology comprising 88 % of stroke. Intracranial hemorrhage makes up an additional 10–15 %, with less common etiologies accounting for the remainder. Mortality rates vary with etiology, with a 38 and 8–12 % 30-day mortality seen in hemorrhagic and ischemic strokes, respectively.

Ischemic Stroke

Ischemia is by far the most common cause of stroke. Ischemic causes can be further subdivided into atherosclerotic, cardiogenic, hemodynamic, or cryptogenic sources. Atherosclerotic causes are the most common subtype as thrombi are formed in vessels with abnormal endothelium, usually directly at atherosclerotic plaque.

Emboli travel distally from the site of origin from the heart or intra-/extracranial vessels. Arterial emboli are often produced at the site of atherosclerotic plaque that dislodge and travel downstream creating an artery-to-artery embolism. Common sites for thromboembolic disease include the carotid bifurcation, carotid siphon, proximal portions of the anterior/middle cerebral arteries, subclavian artery, origin of the vertebral artery, distal vertebral artery, and basilar artery. Cardioembolic events may occur in the setting of relative stasis of blood resulting in thrombus formation within the heart.

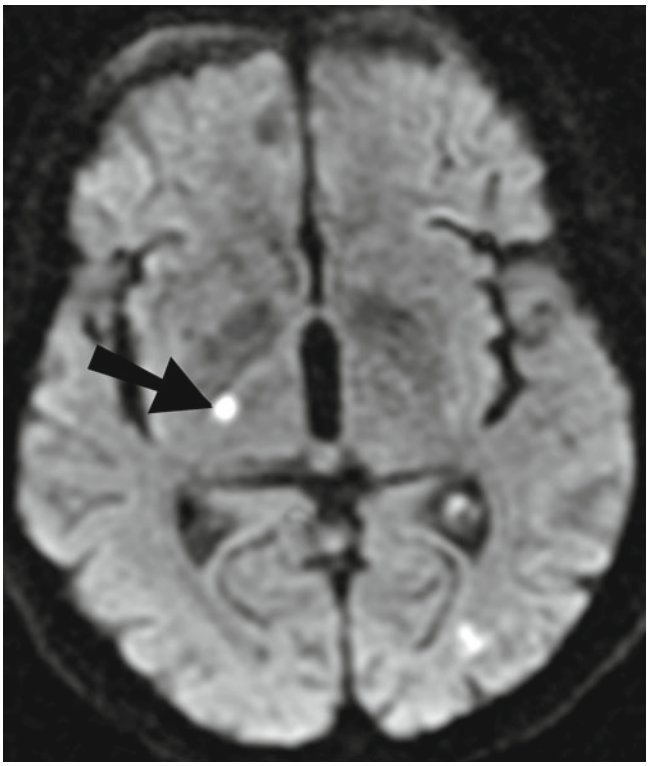

Fig. 18.1 Acute infarct. Diffusion-weighted images showing acute lacunar infarct (*arrow*) in posterior limb of right internal capsule

Occlusion of small perforating end arteries results in lacunar infarcts, which are infarcts less than 15 mm in diameter and frequently occur in the basal ganglia, internal capsule, pons, or corona radiata (Fig. 18.1). Occlusion of terminal branches causes cortical infarcts.

Less common etiologies, representing less than 5 % of acute stroke, include vasculopathies, immune-related diseases, hypercoagulable states, arterial dissection, global hypoperfusion, venous infarction, and mitochondrial disorders.

S.K. Dundamadappa, MD • M. Ehinger, MD • A. Chen, MD (✉)
Department of Radiology, University of Massachussetts,
55 Lake Avenue North, Worcester, MA 01655, USA
e-mail: andrew.chen@umassmemorial.org

A. Singh (ed.), *Emergency Radiology*,
DOI 10.1007/978-1-4419-9592-6_18,

Concept of Penumbra

Once vascular supply to the brain has been compromised, there is a window of opportunity for reversing ischemic symptoms depending upon the level to which the blood flow has dropped. Normal cerebral flow ranges between 60 and 100 ml/100 g/min, with varying degrees of hypoperfusion seen at lower flow rates. Brain parenchyma can compensate for a decrease in perfusion by increasing oxygen extraction to a cerebral blood flow (CBF) of approximately 20–23 ml/100 g/min. While blood flow of 10–20 ml/100 g/min may be reversible for a period of hours, more severe perfusion deficit (below 10 ml/100 g/min) may lead to infarction within minutes. Ischemic brain tissue can functionally be divided into three components – infarct core, penumbra, and oligemic region (Fig. 18.2). When a cerebral artery is occluded, a core of brain tissue with severe perfusion deficit dies rapidly while the surrounding brain tissue (ischemic penumbra) with moderately reduced blood flow that may have lose electrical activity. Tissue in the penumbra may be salvageable with reperfusion; otherwise, the tissue in penumbra will progress to infarction. Mildly reduced blood flow to the oligemic region surrounds the penumbra and is more likely to survive unless perfusion is further hemodynamically altered.

Imaging Workup of Acute Ischemic Stroke

In the past, imaging was primarily used to exclude hemorrhage and evaluate for surgically amenable lesions. The role of imaging has changed dramatically over the last decade and currently involves detection as well as extent of the infarct and penumbra.

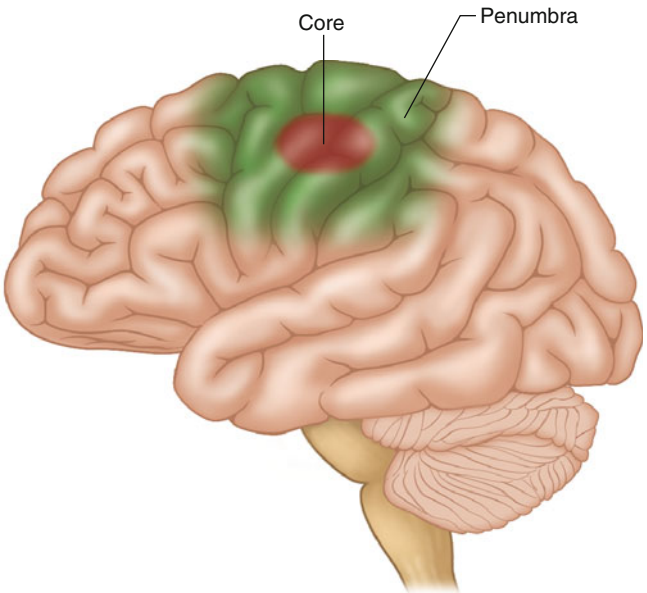

Fig. 18.2 Schematic diagram shows an acute infarct and the surrounding penumbra

Goals in acute stroke imaging are to assess the 4 "Ps" [2]:

Parenchyma: Assess early signs of acute stroke and rule out hemorrhage.

Pipes: Assess extracranial circulation and intracranial circulation for intravascular thrombus, occlusion, and severe stenosis.

Perfusion: Assess cerebral blood volume, cerebral blood flow, and mean transit time (MTT).

Penumbra: Assess tissue at risk of dying if ischemia continues without recanalization.

CT imaging, including noncontrast CT (NCCT), CT angiography (CTA), and CT perfusion (CTP), are the most often the initial imaging modalities in stroke evaluation. At our institution, NCCT followed by CTA is the initial study in stroke evaluation. CTP is performed in select cases to help stratify patients for treatment.

Noncontrast CT

Sensitivity of NCCT is 60–70 % in the first 3–6 h, and virtually all infarcts are seen by 24 h. Despite its relative insensitivity to acute infarcts in the emergency setting, NCCT remains the widely used initial imaging study in acute stroke. It is used to rule out intracranial hemorrhage and other stroke mimics.

CT signs of early ischemia include (Fig. 18.3):

Dense artery sign: Acute thrombus or embolus in a cerebral artery may produce linear hyperdensity in the vessel affected. Hyperdense MCA sign is associated with large MCA territory infarct and is seen in one-thirds of the hyperacute infarcts. MCA "dot" sign refers to hyperdensity in distal MCA and its branches in sylvian fissure.

Loss of gray-white differentiation: In MCA territory infarcts, there is often obscuration of lentiform nucleus (basal ganglia are more sensitive to ischemia due to their end-artery blood supply) and insular ribbon sign (insula is especially sensitive to ischemia due to its distance from collateral flow). Peripherally, acute infarction results in loss of definition of regions of cortex (cortical sign) in the affected vascular territory.

Hypodensity: This becomes more apparent and well circumscribed by 24 h. Variable amount of cerebral swelling develops after 24 h, usually peaks at 3–5 days. The degree of swelling depends on the restoration of flow.

The detection of early acute ischemic stroke on NCCT may be improved by using variable window width and center level settings to accentuate the contrast between normal and edematous tissue [3]. Multiplanar reformats may also help in identifying subtle infarcts (e.g., coronal reformats for superior cerebellar infarcts).

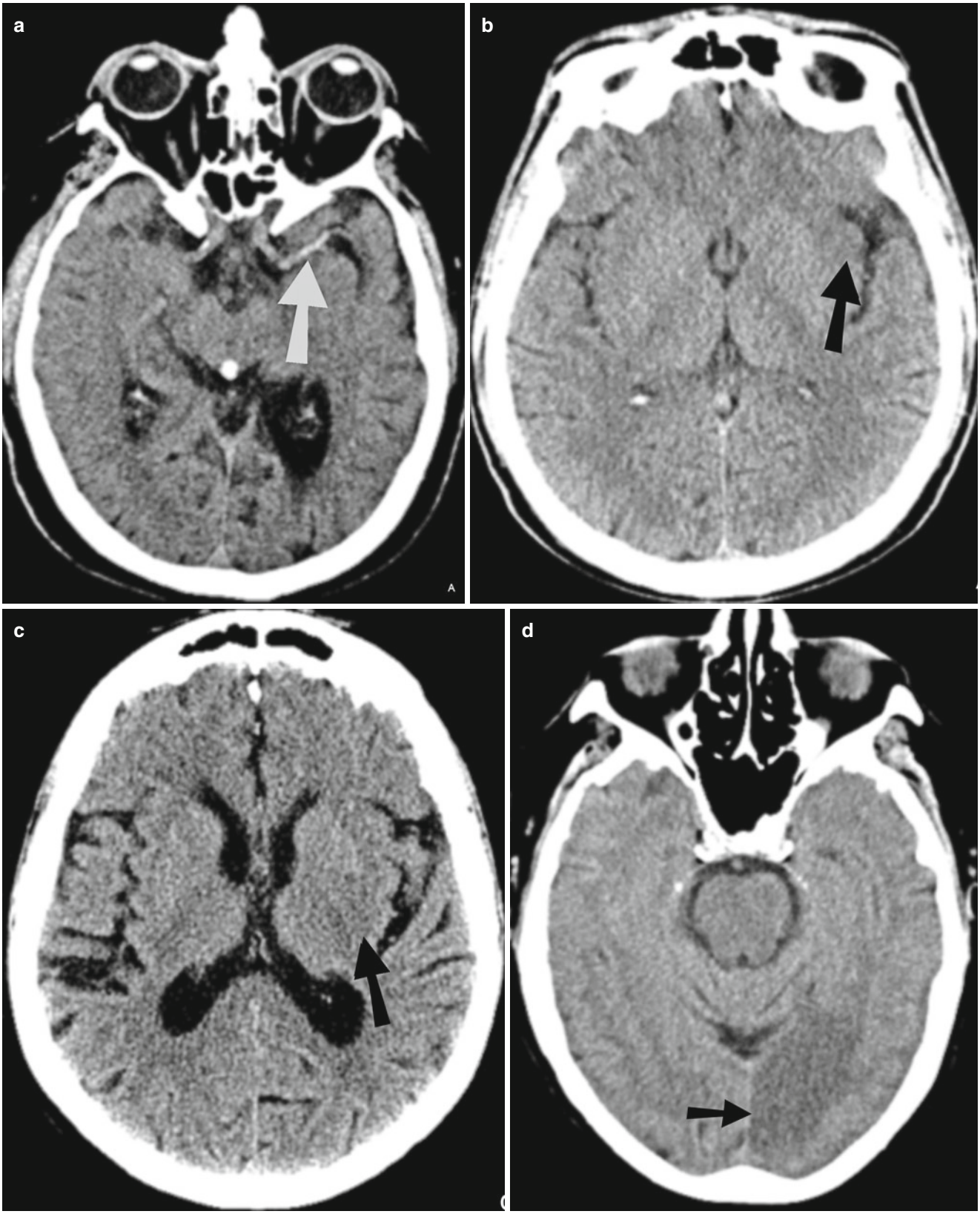

Fig. 18.3 CT signs of acute infarction. (**a**) Noncontrast CT showing hyperdense clot in the left M1 segment (*arrow*) of middle cerebral artery (hyperdense MCA sign). CTA (not shown) confirmed MCA occlusion. (**b**) Noncontrast CT shows loss of grey-white matter differentiation (*arrow*) at the insula (insular ribbon sign). (**c**) Noncontrast CT shows subte hypodensity in posterior aspect of left lentiform nucleus (*arrow*). (**d**) Noncontrast CT shows hypodensity involving both gray and white matter in left occipital lobe (PCA territory) (*arrow*)

CT Angiography

CTA is fast and noninvasive and allows for evaluation of etiology of acute ischemic stroke (such as thrombosis, occlusion, severe stenosis, and dissection). Both source images and 3D images should be reviewed. Though not very accurate, clot morphology like ulceration can also be assessed. When calcified plaques are present, the window can be widened for better evaluation.

CT Perfusion

CTP is a functional imaging technique that can be rapidly performed to evaluate ischemic but potentially salvageable penumbral tissue. CTP is based on the entry and washout of an intravenous iodinated bolus of contrast.

Severely diminished cerebral blood volume (CBV) has been demonstrated as a good correlate to the area of restricted diffusion on MRI and hence is considered a measure of the infarct core. Decreased cerebral blood flow (CBF) and increased mean transit time (MTT) are seen in areas of the brain either at risk for or undergoing infarct. Occasionally, increased CBV (luxury perfusion) may be seen in ischemic region due to autoregulatory vasodilatation and recruitment of collateral vessels. The combination of low CBF and normal/increased CBV represents an area at risk for ischemia (penumbra) but currently compensated by dilated collateral vessels (Fig. 18.4).

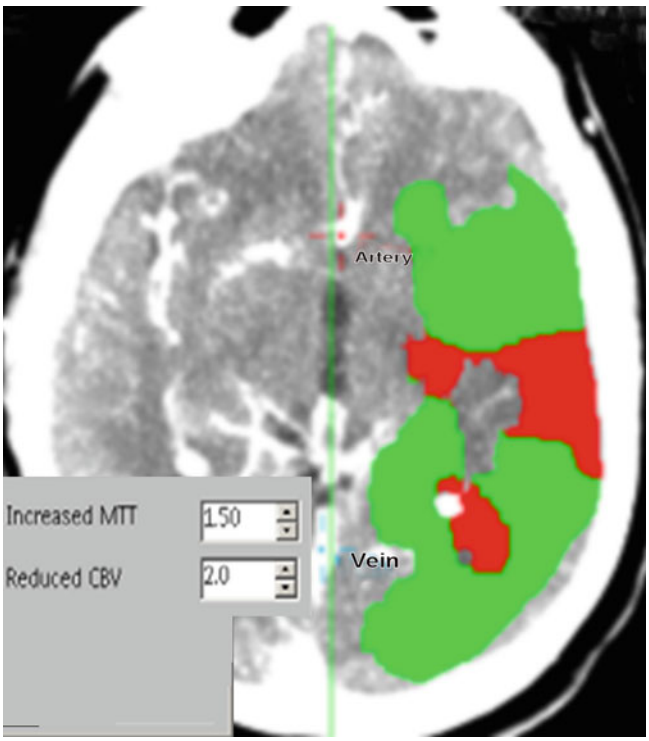

Fig. 18.4 Color-coded summary maps from CT perfusion study showing large penumbra (shown in *green*) in the left MCA territory. The red color indicates severely reduced cerebral blood volume

MR Imaging

MR imaging is more sensitive and specific than CT for detection of acute stroke. The most sensitive imaging sequence for detecting ischemia is diffusion-weighted MR imaging (DWI), with changes in acute infarction detected within minutes of onset of the symptoms. Cytotoxic edema of acute ischemia results in reduced water diffusion in the extracellular matrix. DWI detects this restriction of microscopic motion.

Acute infarct is seen as bright signal intensity on DWI due to restricted diffusion as well as secondary to increased water content (T2 effect), with corresponding decrease on apparent diffusion coefficient (ADC) sequence (Fig. 18.5a). DWI is positive in the acute phase with increasing intensity that peaks at 7 days. The time to normalization of DWI signal has been reported in literature to range from 14 to 72 days [4, 5]. ADC sequence initially has low signal intensity, with maximum hypointensity occurring at 24 h. Signal intensity then increases and normalizes between the 7th and 11th days [6].

Additional findings in acute infarct include the presence of lesion in arterial distribution, hyperintense signal on T2-weighted and fluid-attenuated inversion recovery sequence, subcortical white matter hypointensity on T2-weighted sequence (Fig. 18.5b), exaggerated intravascular enhancement, and findings of vascular occlusion (lack of normal flow void on long TE sequence and high arterial signal on FLAIR sequence related to slow flow/occlusion) (Fig. 18.5c). However, T2 signal can be normal in the first 8 h after ictus. With time, infarcts become hyperintense on T2-weighted sequence, with maximum hyperintensity reached between 7 and 30 days.

MR Perfusion Imaging

MR perfusion imaging techniques include exogenous contrast-enhanced method or an endogenous method (arterial spin labeling). Exogenous dynamic susceptibility-weighted (T2*-weighted) sequence is the most commonly used technique in acute stroke evaluation. The technique involves tracking of the tissue signal loss caused by T2* effects of paramagnetic contrast agent to create a hemodynamic time–signal intensity curve. As in dynamic CT perfusion imaging, various parametric maps (CBV, MTT, CBF, TTP) are calculated from this curve by using a deconvolution technique. The core of infarct demonstrated by restricted diffusion is compared against CBF or MTT maps for mismatch which represents the penumbra, tissue at risk (Fig. 18.6).

Hemorrhagic Transformation

Hemorrhagic transformation of an infarct is a rare (3.6 %) complication in the acute phase. It is thought to be due to reperfusion of ischemic tissue during the first 2 weeks, occurring more commonly in larger infarcts and cardioembolic infarcts. Anticoagulant and thrombolytic agents increase the incidence of hemorrhagic transformation.

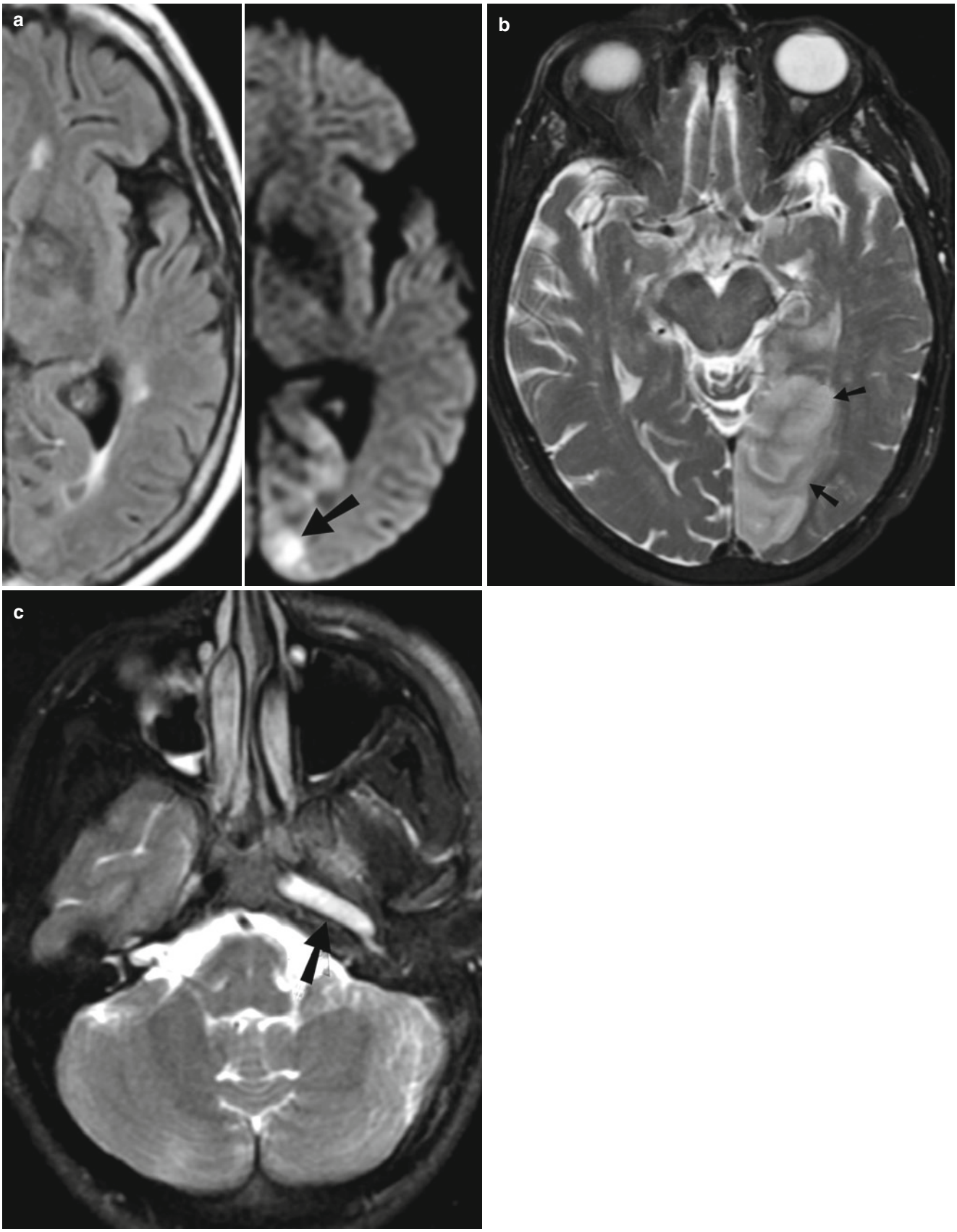

Fig. 18.5 Acute infraction on MRI. (**a**) Acute right PCA territory infarct which is not apparent on T2-weighted sequence, is clearly seen on DWI (*arrow*). (**b**) T2-weighted sequence shows acute left PCA territory infarction (*arrows*). (**c**) Left ICA occlusion: T2-weighted sequence shows hyperintense signal within left ICA (*arrow*), indicating the presence of thrombus in the arterial lumen

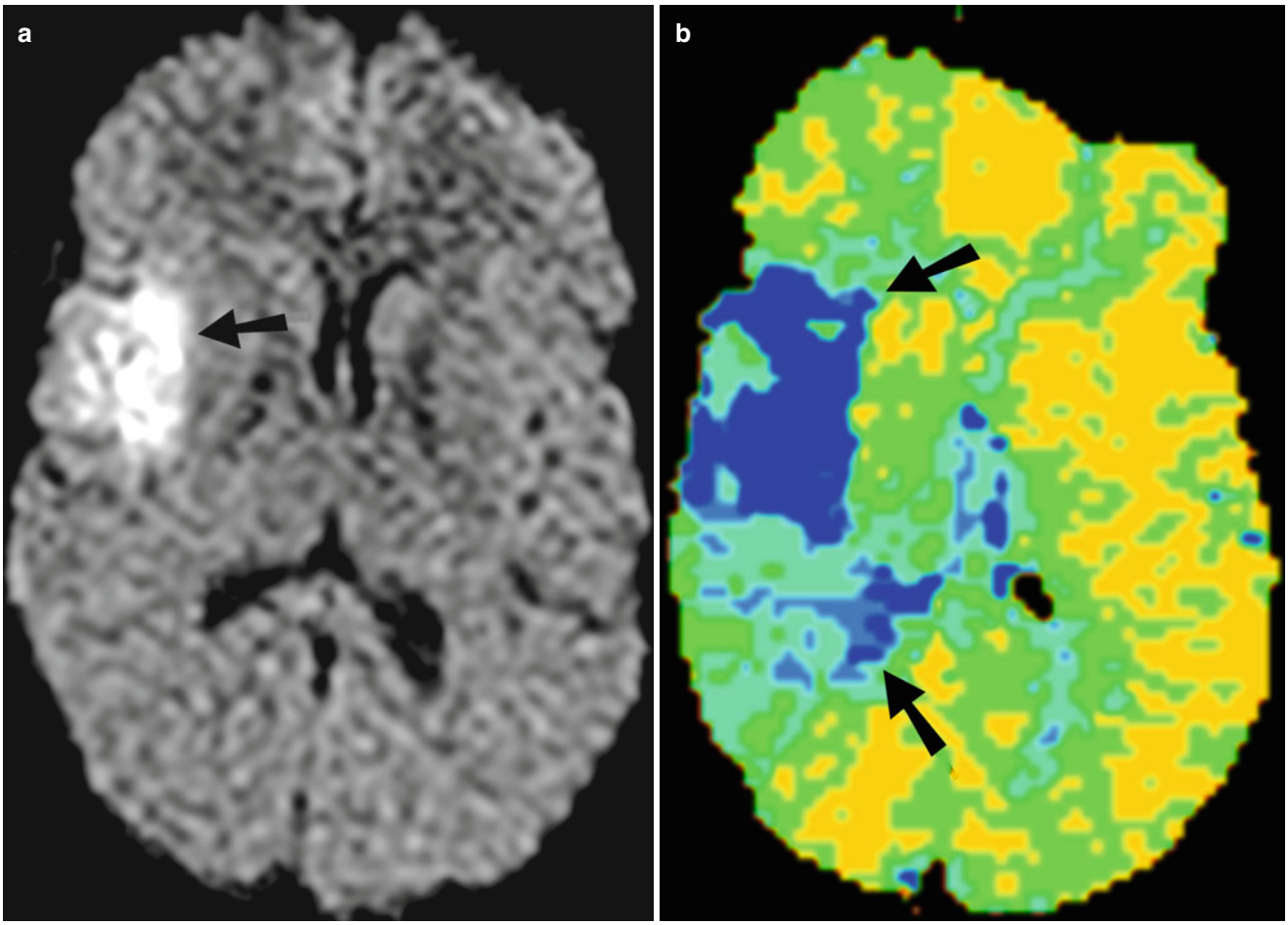

Fig. 18.6 Acute infarction on MR. (**a**) Diffusion-weighted sequence shows a hyperintense acute infarct in the right MCA territory. (**b**) MR perfusion image shows a large defect (*arrows*), suggesting the presence of a penumbra

The European Cooperative Acute Stroke Study (ECASS) classification of hemorrhagic transformation stratified the size of these hemorrhages with the clinical outcome [7].

HI (hemorrhagic infarct) (Fig. 18.7): petechial hemorrhages without space-occupying effect

HI1: small petechiae

HI2: more confluent petechiae

PH (parenchymal hematoma) (Fig. 18.8): hemorrhage (coagulum) with mass effect

PH1: <30 % of the infarcted area with mild space-occupying effect

PH2: >30 % of the infarcted area with significant space-occupying effect

Only PH2 independently modifies the risk of a worse clinical outcome both early and late after stroke onset. PH-1 has increased risk of early deterioration but not of a worse long-term outcome. HI is not associated with worse early or late outcome [8].

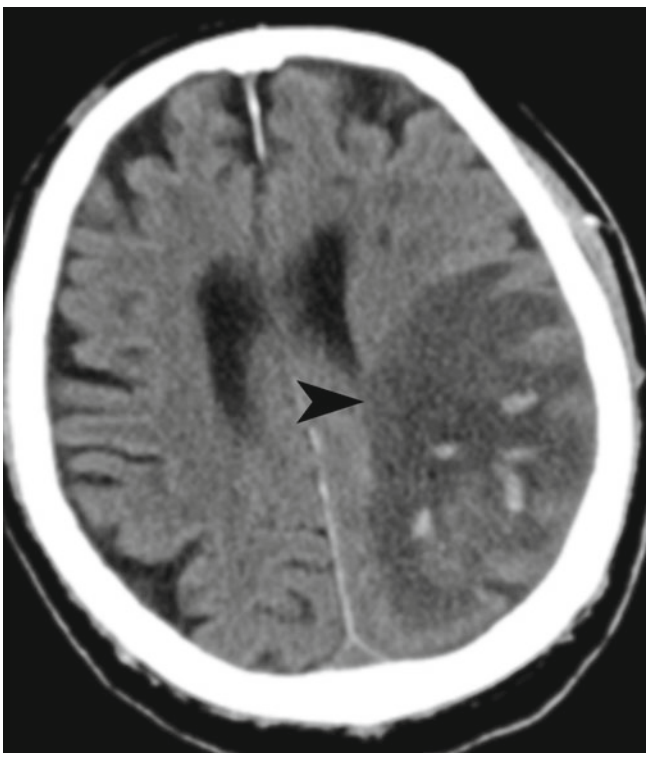

Fig. 18.7 Acute infarct with hemorrhage. Noncontrast CT shows petechial hemorrhages with left parietal infarct (*arrowhead*) (ECASS HI2)

Infarction from Septic Emboli

This is a subset of embolic infarctions, mostly seen with intravenous drug abuse, infective endocarditis, and cardiac valve abnormalities. The most common MRI finding in early stages of septic emboli is that of ordinary embolic infarction. Eventually changes related to infection show up, with disproportionate edema, enhancement, cerebritis, and finally frank abscess formation. Like other embolic infarctions, these show a higher tendency to bleed.

Fig. 18.8 Acute infarct with hemorrhage. Noncontrast CT shows intraparenchymal as well as intraventricular hemorrhage (*arrow*) within left MCA territory infarction (ECASS PH2), following IV tPA

Watershed Infarction

Watershed or boundary zone infarctions occur from hypoperfusion at the junction between arterial territories and have two patterns (Fig. 18.9):

Superficial border zone: These are infarctions of the cortex and adjacent white matter located at the boundary zone between leptomeningeal collaterals from adjacent arterial territories (ACA/MCA, MCA/PCA, and ACA/PCA).

Internal border zone: They occur in the corona radiata and centrum semiovale, between lenticulostriate perforators and the deep-penetrating cortical branches of the MCA and between deep white matter branches of the MCA and the ACA.

Infarct Evolution

Subacute stage approximately extends from 2 to 14 days following the initial ischemic event. In this stage the infarcts become better circumscribed. Mass effect peaks by 3–5 days and then diminishes. When there is hemorrhagic transformation, MR signal characteristics of blood change with age. Contrast enhancement seen typically in this stage can be gyral or patchy (Fig. 18.10). It typically begins toward the

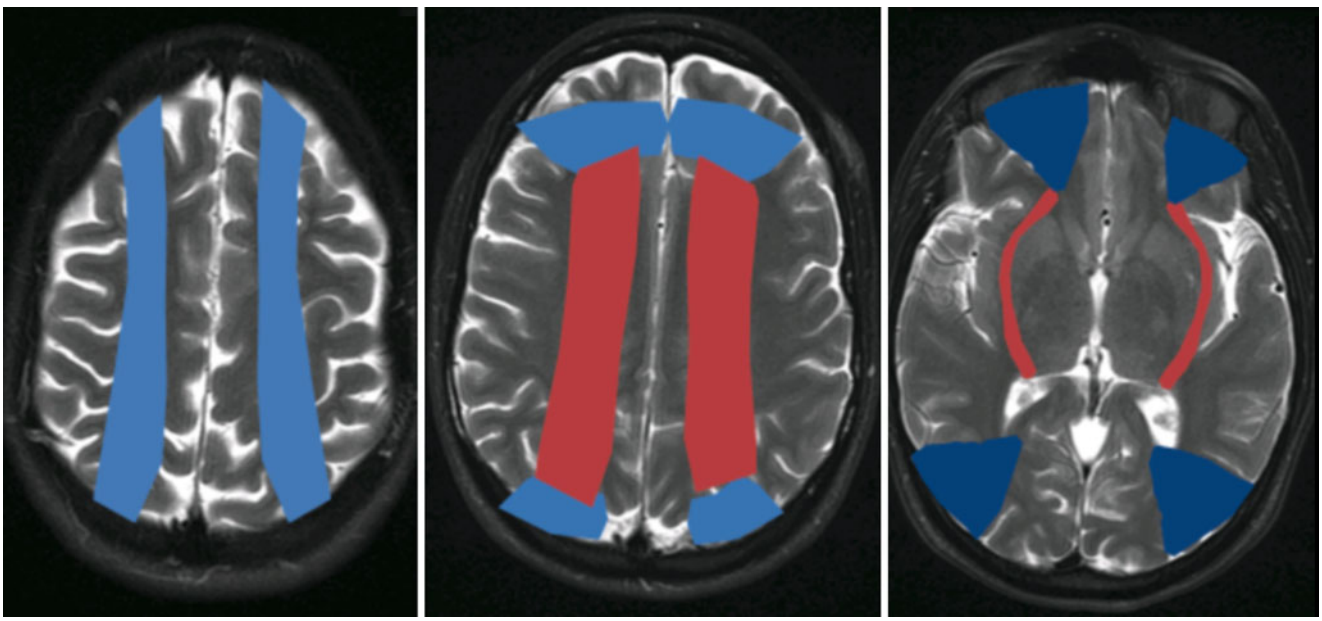

Fig. 18.9 Schematic representation of the superficial (*colored red*) and internal (*colored blue*) watershed zones in the cerebral hemispheres

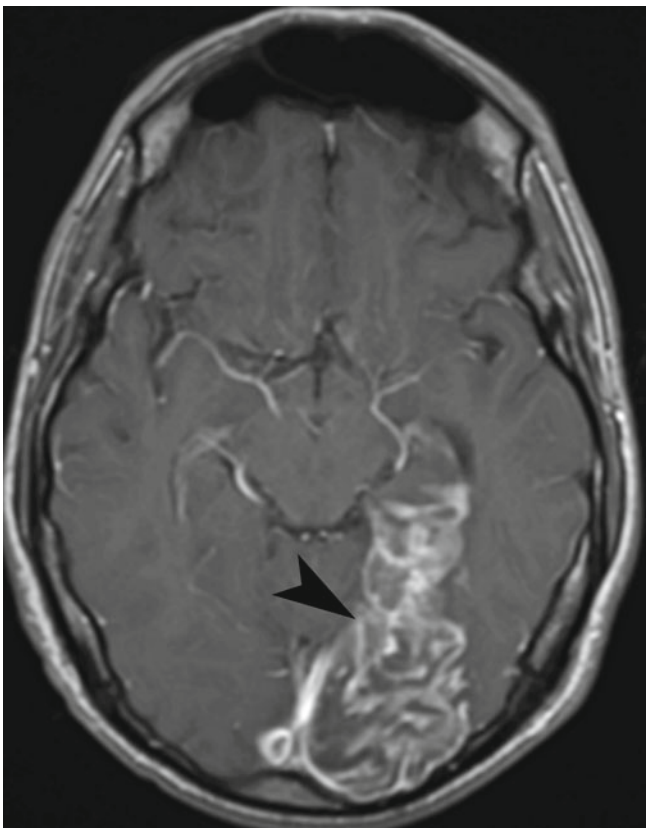

Fig. 18.10 Subacute infarction on MR. Contrast-enhanced T1-weighted image showing enhancing subacute infarct in left PCA territory (*arrowhead*)

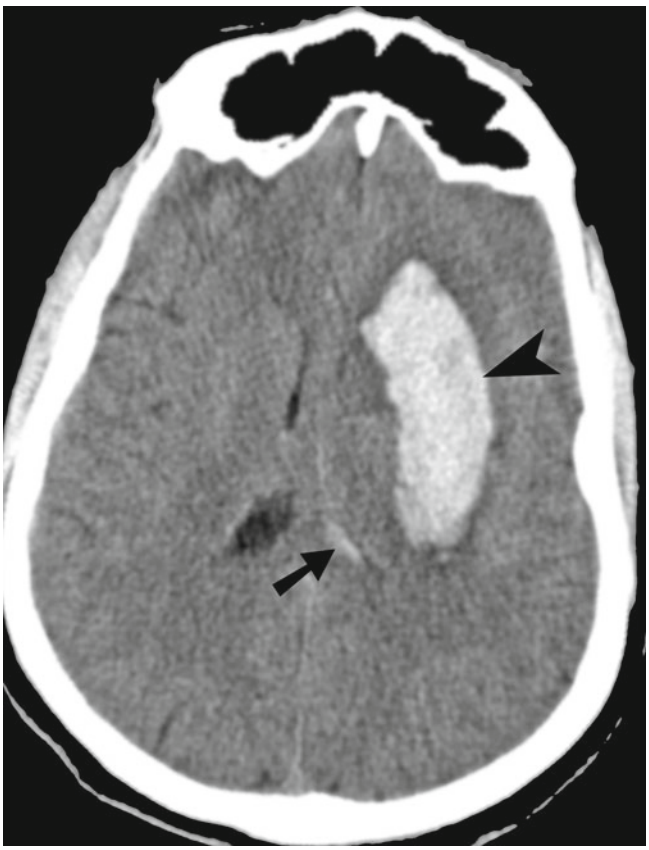

Fig. 18.11 Hypertensive hemorrhage. Noncontrast CT of the head demonstrates intraparenchymal hypertensive hemorrhage (*arrowhead*) in the left basal ganglia region with small intraventricular extension (*arrow*)

end of the first week, when mass effect has resolved, and persists for approximately 6–8 weeks. This discordance between enhancement and mass effect is a useful radiologic observation, because enhancing lesions with significant mass effect is unlikely to represent cerebral infarction [9].

The chronic stage of cerebral infarction begins weeks to months after the initial ischemic event, when the integrity of the blood–brain barrier is restored and edema has resolved. The infarcts are smaller and better defined than seen in earlier stages and no longer enhance. Gliosis or encephalomalacia and volume loss are the hallmarks of this stage.

Posttreatment Imaging

After treatment, CT is generally used to evaluate infarct progression or look for posttreatment hemorrhagic conversion. Special attention is paid to history and timing of any previous angiographic intervention, as dense contrast from this procedure can mimic blood.

Nontraumatic Intracranial Hemorrhage

Nontraumatic intracranial hemorrhage (ICH) accounts for about 15 % of strokes in the USA. The hemorrhages are typically parenchymal or subarachnoid but may be subdural, intraventricular, or rarely epidural. Further discussion in this section is limited to parenchymal hemorrhage.

Etiology

The causes of nontraumatic and noninfarct-related parenchymal ICH include hypertension, vascular malformations, amyloid angiopathy, neoplasm, coagulopathies, drug abuse, anticoagulants, thrombolytics, and venous thrombosis. Rarer causes like vasculitis and reversible cerebral vasoconstrictive syndrome can also be considered.

Hypertension is the most prevalent and modifiable risk factor for spontaneous ICH. The most frequent anatomic locations for hypertensive ICH are the putamen (Fig. 18.11),

globus pallidus, external capsule, subcortical white matter, thalamus, internal capsule, and in the cerebellum and brain stem.

Cerebral amyloid angiopathy refers to the deposition of β-amyloid in small- and midsized arteries (and less frequently veins) of the cerebral cortex and the leptomeninges. Its prevalence is approximately 5–8 % in people in the seventh decade and 55–60 % of people who are 90 years or older [10]. It has been reported to account for 5–20 % of nontraumatic cerebral hemorrhages in elderly patients [11]. The hemorrhages are typically lobar (parietooccipital predominance) of different ages and affect elderly normotensive patients.

In a population-based study, 12 % of all cases of ICH were on anticoagulation medications at the time of their hemorrhage, compared with only 4 % of age-, race-, and gender-matched control [12].

Vascular malformations are the leading cause of spontaneous ICH in young adults. Arteriovenous malformations (AVM) and cavernous malformations (CM) account for most of the clinically evident hemorrhages. Brain tumors may have associated ICH, in up to 15 % of patients, but rarely is hemorrhage the presenting symptom of a previously undiagnosed brain mass [13]. Hemorrhagic primary brain tumors are generally high-grade tumors like glioblastoma multiforme and anaplastic astrocytoma. The intracerebral metastases that are most likely to hemorrhage are those caused by choriocarcinoma, melanoma, thyroid carcinoma, and renal cell carcinoma. However, most hemorrhagic metastases are caused by breast and lung carcinomas, as they are more common causes of brain metastases in the general population.

Illicit drugs associated with ICH include cocaine, amphetamines, phenylpropanolamine, phencyclidine, ephedrine, and pseudoephedrine. The predominant underlying mechanism is abrupt hypertension or in some cases vasculitis.

Hemorrhage from cerebral venous thrombosis is typically cortical in location, with subcortical extension [14]. Flame-shaped irregular zones of lobar hemorrhage in the parasagittal frontal and parietal lobes are typical findings in superior sagittal sinus thrombosis, whereas hemorrhage in the temporal or occipital lobes is more typical of transverse sinus thrombosis.

Imaging Evaluation

Noncontrast CT of the head is generally the initial investigation given the wide availability and high sensitivity for acute hemorrhage. Acute hematoma is hyperdense on CT with density between 50 and 70 Hounsfield units. After the third day, the blood density gradually decreases from periphery to the central region. CT also provides information on the location, size, intraventricular extension, mass affect, hydrocephalus, or midline shift.

Table 18.1 MR findings of hemorrhagic products

Stage of hematoma	Time	Signal on T1WI	Signal on T2WI
Hyperacute	First 6 h	Low	High
Acute	Up to 3 days	Iso to low	Low
Early subacute	4–7 days	High	Low
Late subacute	1 week to several months	High	High
Chronic	Months to years	Low	Low

Contrast-enhanced MR imaging is the next imaging step in the subset of patients to evaluate for an underlying lesion. MR imaging of hemorrhage is more complex than CT, and the signal characteristics of the hematoma vary with its age (Table 18.1). Gradient-recalled echo or susceptibility-weighted sequences are sensitive for the detection of hemorrhage. Five stages of hemorrhage can be identified by MRI.

An important role of imaging is to evaluate for an underlying lesion. Heterogeneity of the hematoma (Fig. 18.12), enhancing component, hypodense filling defect on CT (Fig. 18.13), disproportionate surrounding edema, unusual or lobar location, unusual age, known primary tumor, additional enhancing lesions, abnormal calcification, and incomplete peripheral hypointense rim on T2 images suggest an underlying mass lesion. Contrast-enhanced MRI is more sensitive in detection of enhancing tumor component in or adjacent to the hematoma. Follow-up imaging may show delayed evolution of blood breakdown products, persistent edema, mass effect, or serpiginous flow voids. The underlying lesion may become more apparent as the hematoma resolves.

Underlying vascular malformation may be suggested by younger age of the patient and prominent vessels or linear calcification adjacent to the hematoma (Fig. 18.14). Catheter angiography is used to diagnose small AVMs that may be occult on both CT and MR, to fully characterize an AVM, and to perform therapeutic intervention. Repeat angiography after resorption of the hematoma is appropriate in selected patients with a high index of suspicion and a negative initial cerebral angiogram [11]. Cavernomas show characteristic "popcorn ball" morphology on MRI with complete T2 hypointense rim.

The direct signs of cerebral venous thrombosis can be seen on noncontrast CT (sensitivity of about 33 %) and include visualization of hyperattenuating thrombus in dural sinus (dense clot sign) (Fig. 18.15) [15]. The "cord sign" represents direct visualization of a hyperattenuating thrombosed cortical vein. Given this limited sensitivity of noncontrast CT, if the location of hematoma or the clinical features raise the possibility of venous thrombosis, further evaluation

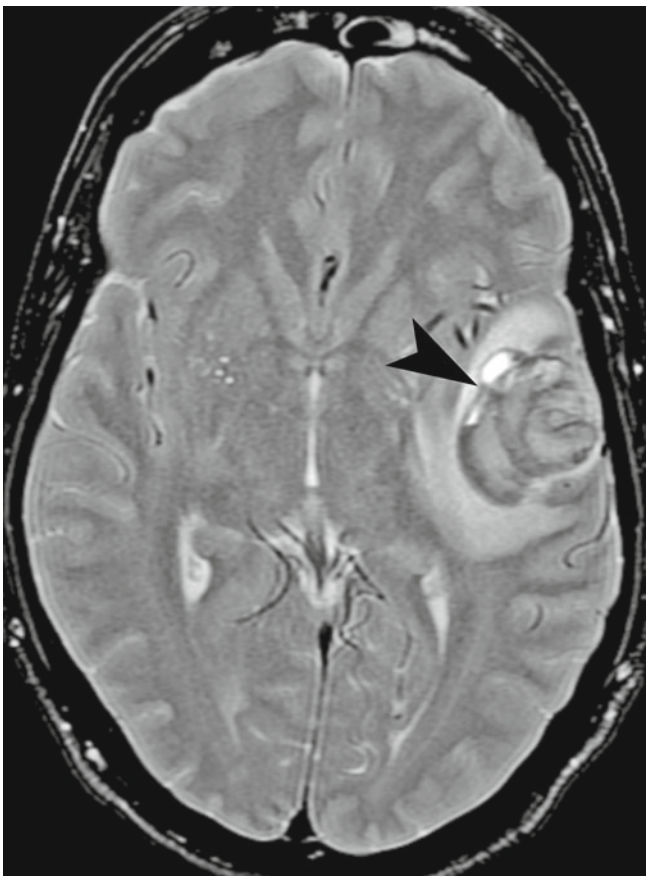

Fig. 18.12 Hemorrhagic primary intracranial tumor. T2-weighted image shows marked heterogeneity (*arrowhead*) of the hematoma in a patient with hemorrhagic glioblastoma multiforme

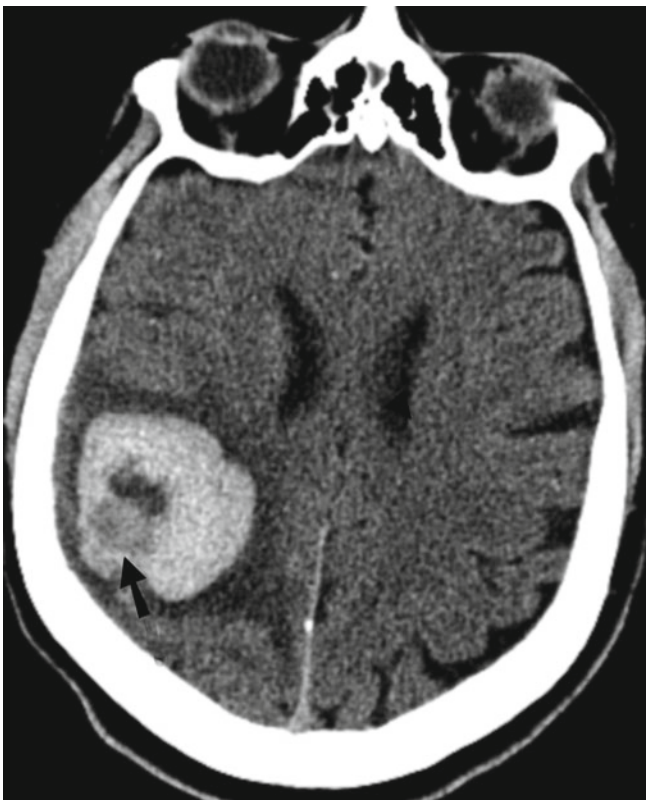

Fig. 18.13 Hemorrhagic metastatic melanoma. Noncontrast CT shows eccentric mass within the hematoma (*arrow*) in a patient with known melanoma

should be done by MRI and MRV or CTV. Contrast-enhanced CT can show "the empty delta sign," which represents the filling defect (non-enhancing thrombus) surrounded by the enhancing dural sinus wall. On MRI, thrombosed veins bloom on gradient-recalled images. There may also be intraluminal abnormal signal in the vein depending on the stage of the thrombus. Venographic techniques better demonstrate the thrombus and also show venous collaterals and resultant adjacent dural enhancement. Catheter angiogram can be done for confirmation and intervention.

Subarachnoid Hemorrhage

Subarachnoid hemorrhage (SAH) is most commonly of nontraumatic etiology, occurring secondary to ruptured aneurysm. Less common causes include AVM, vasculitis, venous

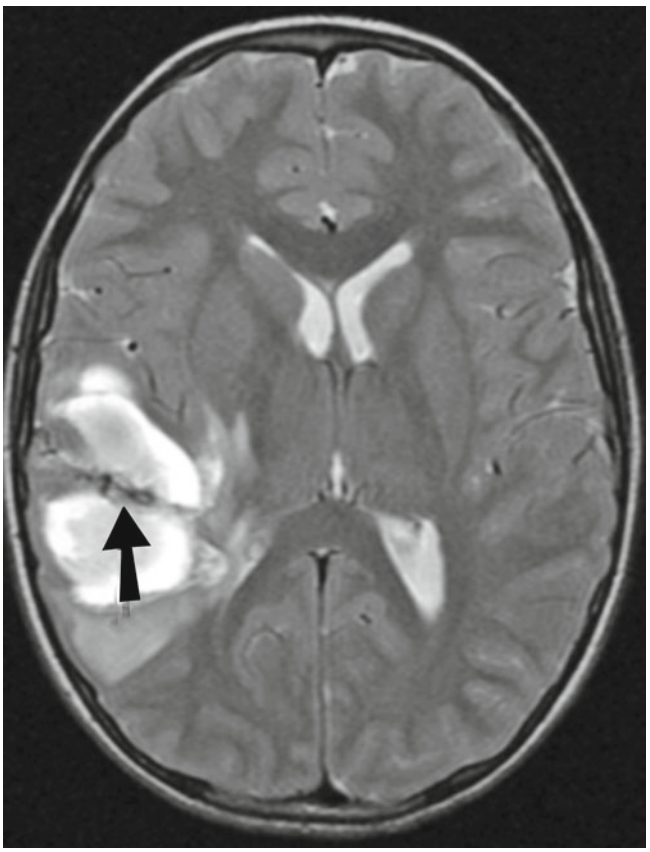

Fig. 18.14 Hemorrhagic AVM. T2-weighted sequence shows hyperintense subacute hematoma. Flow voids from vessels (*arrow*) is seen within the hematoma, suggests the presence of an underlying vascular abnormality

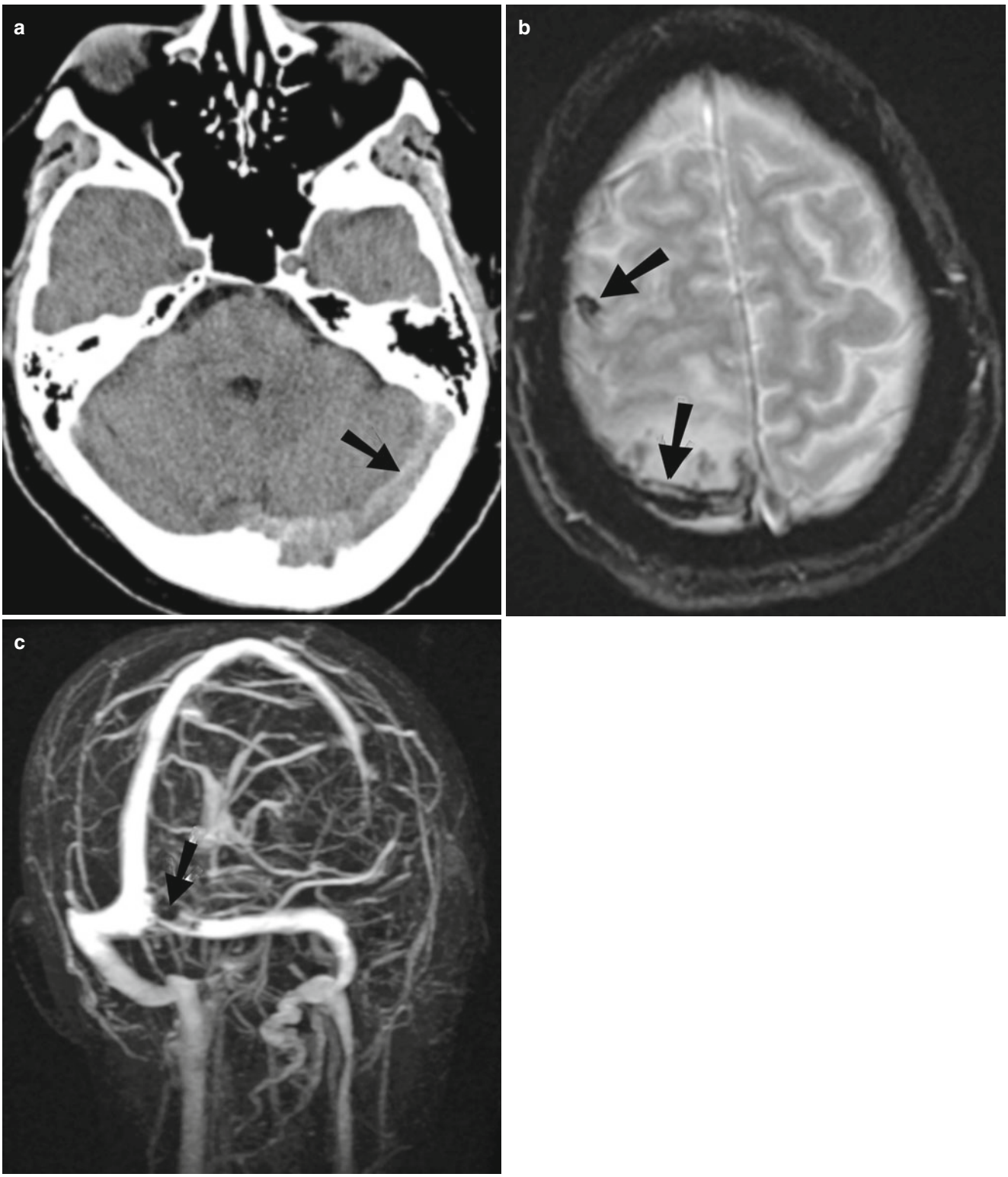

Fig. 18.15 Venous thrombosis, different patients. (**a**) Noncontrast CT shows hyperdense left transverse sinus, (*arrow*), secondary to thrombosis. (**b**) Gradient echo T2-weighted MR sequence shows blooming of thrombosed cortical veins (*arrows*). (**c**) MR venogram shows a focal filling defect within proximal left transverse sinus, from intraluminal thrombus

thrombosis, reversible cerebral vasoconstriction syndrome, and extension of parenchymal/intraventricular hemorrhage into subarachnoid space [16]. Saccular aneurysm is the most common type of cerebral aneurysm. Fusiform aneurysms are less common and are most often the result of atherosclerosis and dissection or found in association with congenital

conditions. Septic emboli may result in mycotic aneurysms which are typically small and located in distal arterial branches. Aneurysms can be seen in feeding arteries, nidus, or draining veins of AVM.

Aneurysms are considered to be acquired lesions, occurring most frequently at the vascular bifurcations. The common locations of aneurysms are anterior communicating artery, clinoid/supraclinoid ICA, middle cerebral artery bifurcation or trifurcation, basilar artery (tip and the origin of superior cerebellar arteries), and vertebral artery (at the origin of the posterior inferior cerebellar arteries). Incidence of unruptured aneurysm is about 5 % [17]. When the aneurysms are multiple, the distribution of SAH and irregular/lobulated contour of the aneurysm is helpful in determining the ruptured aneurysm.

Approximately 10–15% of patients with SAH secondary to aneurysm rupture die before reaching the medical care and 25 % of the rest die over the succeeding 2 weeks [18]. The risk of rebleeding in untreated aneurysm is about 4 % within the first 24 h, 20 % within 2 weeks, and 50 % within 1 month [19].

Imaging Evaluation

The cornerstone of the diagnosis is a noncontrast head CT which has a diagnostic yield of approximately 90 %. SAH is seen as diffuse hyperdensity in subarachnoid space (Fig. 18.16). If hemorrhage is brisk, focal hematoma may form in the subarachnoid space. Careful attention should be paid to areas where a small amount of blood can be easily overlooked, such as posterior aspects of the sylvian fissures, interpeduncular cistern, deep cerebral sulci, occipital horns of the lateral ventricles, and the foramen magnum.

Exuberant inflammatory exudates in the subarachnoid space and recent iodinated contrast administration can result in subarachnoid hyperdensity and mimic SAH. Diseases causing diffuse cerebral edema as well as intracranial mass lesions and severe obstructive hydrocephalus can result in an appearance similar to SAH due to apposition of pial surfaces and resultant engorgement of pial veins [20].

Distribution of SAH, focal clot in subarachnoid space, and parenchyma hematoma may help in localization of ruptured aneurysm on NCT. The aneurysm may be seen as a

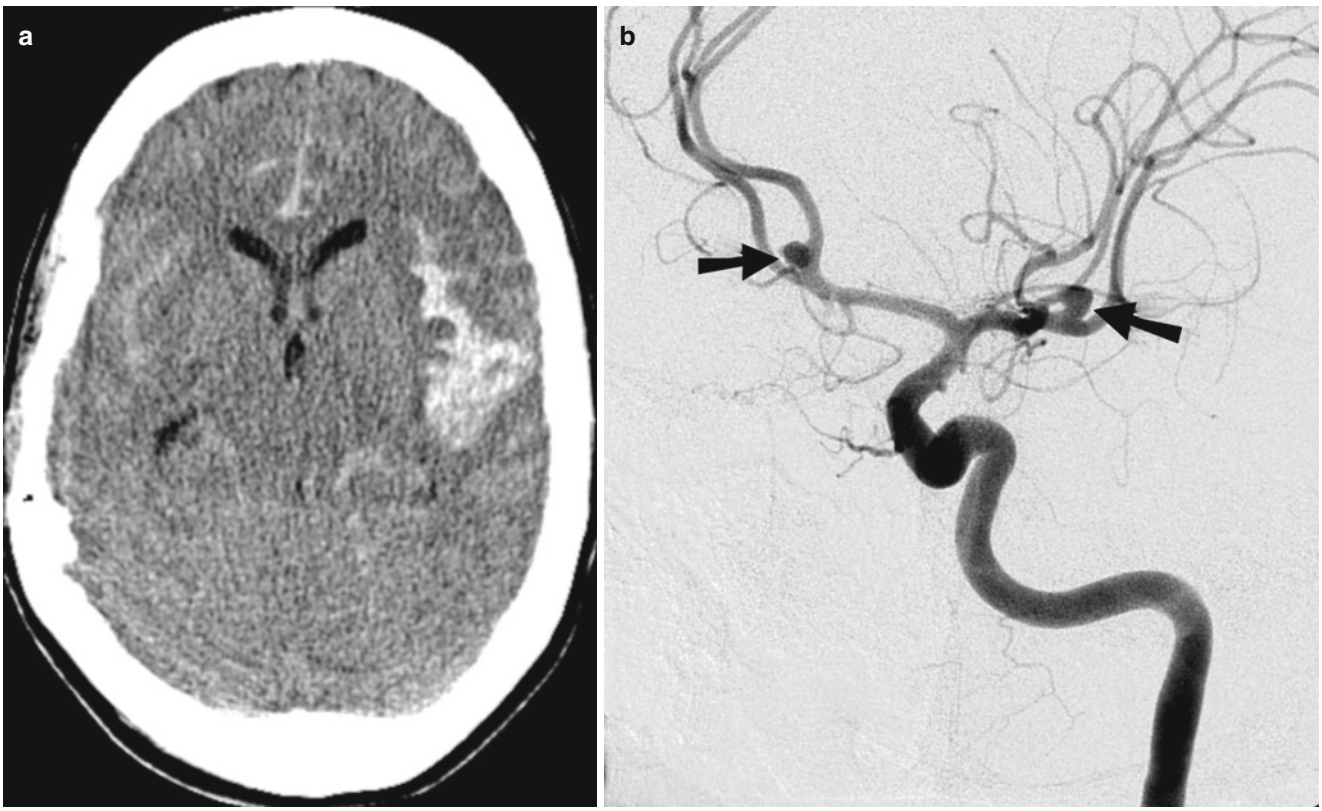

Fig. 18.16 Subarachnoid hemorrhage from ruptured circle of Willis aneurysm. (**a**) Noncontrast shows bilateral subarachnoid hemorrhage, most prominently involving the left sylvian fissure. (**b**) Subsequent digital subtraction angiogram shows left MCA and anterior communicating artery aneurysms (*arrows*). Given the focal hematoma in left sylvian fissure and lobulated contour, left MCA aneurysm is likely the source of bleeding

relatively hypodense area within the dense SAH. On CT, SAH generally resolves by 5–7 days. Smaller bleeds may resolve earlier. Focal clot, if present, may persist for a longer time.

Generally a lumbar puncture is performed to evaluate for xanthochromia in patients who have suspected SAH and a negative CT scan. Xanthochromia is representative of the presence of bilirubin in the CSF and requires at least 12 h to develop [18].

Computed Tomography Angiography (CTA)

CTA is generally the next investigation in SAH evaluation. The sensitivity of multidetector CTA is reported to be 94.8 % and the specificity 95.2 % for the detection on a per aneurysm basis and 99.0 and 95.2 % on a per patient basis, respectively [21]. In this study, a cutoff size of 2 mm was found as the inflection point at which CTA became less able to detect aneurysms. CTA demonstrates the location of aneurysm and evaluates for the presence of thrombus and wall calcification.

MRI

SAH has different MR imaging features than other intracranial hemorrhages. This is due to mixing of blood with CSF and resultant dilution, antifibrogenic elements in CSF and relatively high oxygen saturation of CSF (which limits amount of paramagnetic deoxyhemoglobin) [17]. Due to relative lack of magnetic inhomogeneity of SAH, gradient-recalled images are less sensitive for the detection SAH. T2-weighted fluid-attenuated inversion recovery (FLAIR) is the most sensitive sequence for SAH and shows subarachnoid hyperintensity. Larger amount of blood can demonstrate blooming on gradient-recalled images. Also, T1 images may show slight inhomogeneity of CSF with mild hyperintensity. FLAIR is comparable in its sensitivity to CT in detection of acute SAH. In our experience it is better than CT in subacute stage (Fig. 18.17). However, FLAIR is prone to artifacts, especially in the posterior fossa and adjacent to metallic hardware. Also other leptomeningeal inflammatory and neoplastic processes can result in subarachnoid hyperintensity in FLAIR images. SAH also causes reactive contrast enhancement in the meninges.

Magnetic Resonance Angiography (MRA)

The reported sensitivity of MRA in the detection of aneurysms 3 mm or larger is 90 %, but this number falls precipitously for smaller aneurysms with reported sensitivity of less than 40 %. MRA may be impractical in acute settings as most of the patients are ill and may not be able to lay still. This is a good modality to follow up unruptured aneurysms.

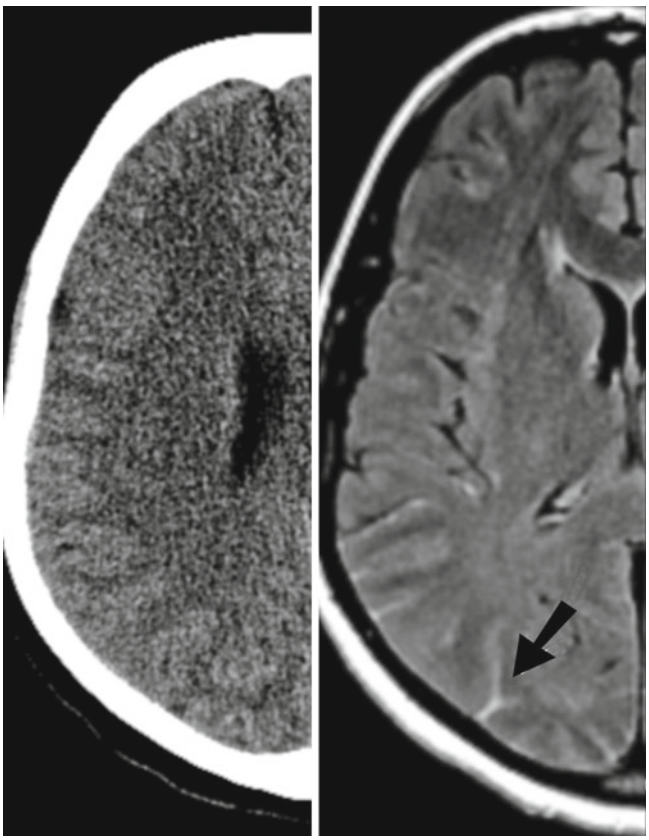

Fig. 18.17 Subacute SAH. Noncontrast CT fails to show sulcal hyperdensity, but FLAIR image clearly shows sulcal hyperintensity from subarachnoid hemorrhage (*arrow*)

Catheter Angiogram

This is the gold standard for aneurysm evaluation. If there is high suspicion for SAH and the noninvasive imaging fails to show an aneurysm, DSA should be done for further evaluation.

Angiogram can be negative in up to 10 % SAH, possibly due to vasospasm or clot filling up the aneurysm. A repeat catheter angiogram is usually performed at about the 7th day to look for aneurysms missed on the first study.

Vasospasm

After initial treatment and diagnosis of SAH, clinical deterioration can occur due to recurrent hemorrhage, hydrocephalus, vasospasm, and stroke. Vasospasm represents the leading cause of mortality and usually begins approximately 3 days after the initial bleed [17]. The proposed causes of SAH include reactive vasoconstriction, decreased vascular autoregulation, reversible vasculopathy, and relative hypovolemia [22].

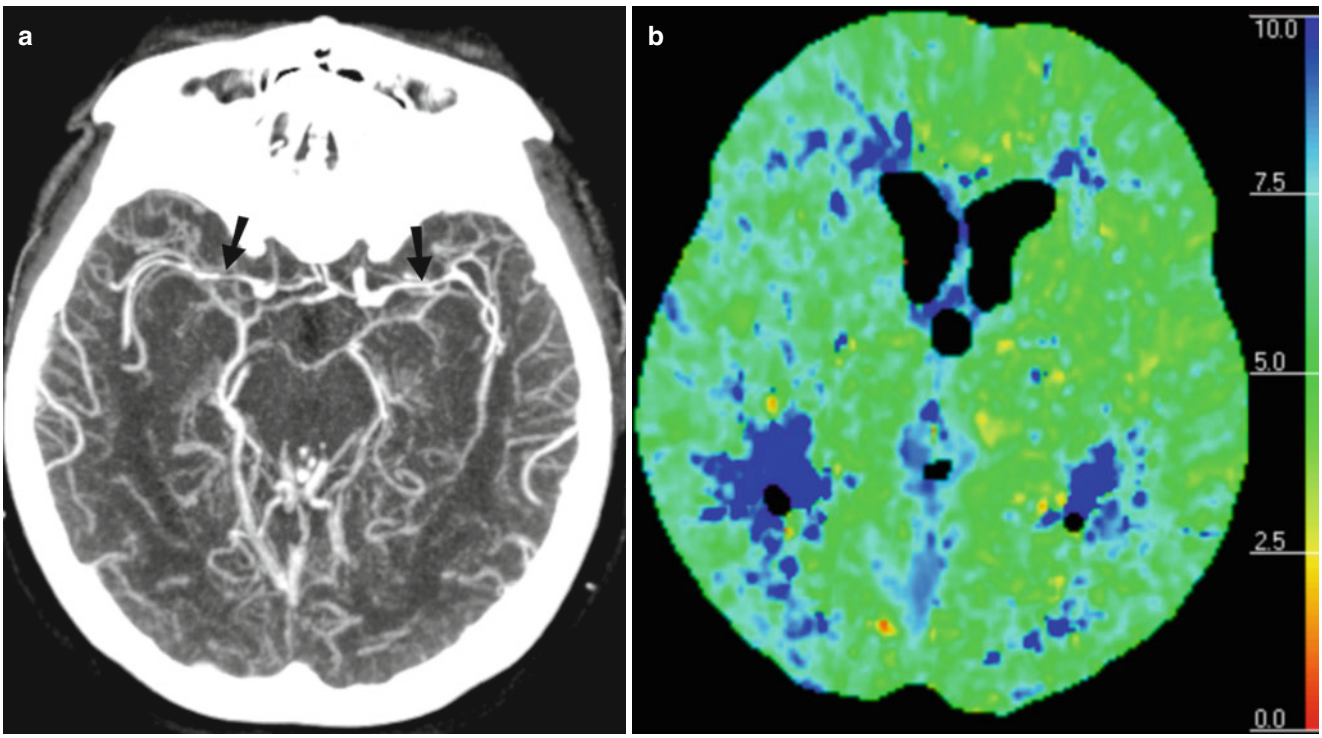

Fig. 18.18 Intracranial vasospasm. (**a**) CT angiogram shows vasospasm in bilateral middle cerebral arteries (*arrows*) and bilateral proximal posterior cerebral arteries. (**b**) Mean transit time (MTT) map from CT perfusion study shows prolonged MTT, more so on the left

The radiologic findings often precede such clinical deficits and thus offer the opportunity to potentially intervene to prevent neurologic injury.

The methods for diagnosing vasospasm include transcranial Doppler (TCD) ultrasonography, CTA, CTP, and DSA (gold standard). The validity of TCD as a monitor for VS has been controversial and is best, an adjunct to other tests. CTA has relatively good sensitivity and specificity in discovering severe VS of proximal arteries (Fig. 18.18a). It also has a high negative predictive value. MTT is reported to be the most accurate perfusion CT parameter for the diagnosis of vasospasm (Fig. 18.18b) [21]. DSA is the gold standard for diagnosis of vasospasm. Endovascular treatment options for vasospasm include intra-arterial vasodilator and angioplasty.

Stroke imaging has made significant progress in the last several years and is evolving. With technologic advances, together with better anatomic depiction, increased emphasis will be on functional imaging to determine tissue viability and the appropriateness of therapy.

References

1. Lloyd-Jones D, Adams RJ, Brown TM, Carnethon M, Dai S, De Simone G, et al. Executive summary: heart disease and stroke statistics–2010 update: a report from the American Heart Association. Circulation. 2010;121(7):948–54.
2. Rowley HA. The four ps of acute stroke imaging: parenchyma, pipes, perfusion, and penumbra. AJNR Am J Neuroradiol. 2001; 22(4):599–601.
3. Srinivasan A, Goyal M, Al Azri F, Lum C. State-of-the-art imaging of acute stroke. Radiographics. 2006;26 Suppl 1:S75–95.
4. Burdette JH, Ricci PE, Petitti N, Elster AD. Cerebral infarction: time course of signal intensity changes on diffusion-weighted MR images. AJR Am J Roentgenol. 1998;171(3):791–5.
5. Huang IJ, Chen CY, Chung HW, Chang DC, Lee CC, Chin SC, et al. Time course of cerebral infarction in the middle cerebral arterial territory: deep watershed versus territorial subtypes on diffusion-weighted MR images. Radiology. 2001;221(1):35–42.
6. Eastwood JD, Engelter ST, MacFall JF, Delong DM, Provenzale JM. Quantitative assessment of the time course of infarct signal intensity on diffusion-weighted images. AJNR Am J Neuroradiol. 2003;24(4):680–7.
7. Hacke W, Kaste M, Fieschi C, Toni D, Lesaffre E, von Kummer R, et al. Intravenous thrombolysis with recombinant tissue plasminogen activator for acute hemispheric stroke. The European Cooperative Acute Stroke Study (ECASS). JAMA. 1995;274(13):1017–25.
8. Berger C, Fiorelli M, Steiner T, Schabitz WR, Bozzao L, Bluhmki E, et al. Hemorrhagic transformation of ischemic brain tissue: asymptomatic or symptomatic? Stroke. 2001;32(6):1330–5.
9. Atlas SW. Magnetic resonance imaging of the brain and spine. Philadelphia: Lippincott Williams & Wilkins; 2008.
10. Masuda J, Tanaka K, Ueda K, Omae T. Autopsy study of incidence and distribution of cerebral amyloid angiopathy in hisayama, Japan. Stroke. 1988;19(2):205–10.
11. Fischbein NJ, Wijman CA. Nontraumatic intracranial hemorrhage. Neuroimaging Clin N Am. 2010;20(4):469–92.
12. Woo D, Sauerbeck LR, Kissela BM, Khoury JC, Szaflarski JP, Gebel J, et al. Genetic and environmental risk factors for intracerebral hemorrhage: preliminary results of a population-based study. Stroke. 2002;33(5):1190–5.

13. Salmaggi A, Erbetta A, Silvani A, Maderna E, Pollo B. Intracerebral haemorrhage in primary and metastatic brain tumours. Neurol Sci. 2008;29 Suppl 2:S264–5.
14. Leach JL, Fortuna RB, Jones BV, Gaskill-Shipley MF. Imaging of cerebral venous thrombosis: current techniques, spectrum of findings, and diagnostic pitfalls. Radiographics. 2006;26 Suppl 1:S19–41; discussion S42–3.
15. Poon CS, Chang JK, Swarnkar A, Johnson MH, Wasenko J. Radiologic diagnosis of cerebral venous thrombosis: pictorial review. AJR Am J Roentgenol. 2007;189(6 Suppl): S64–75.
16. Linn FH, Rinkel GJ, Algra A, van Gijn J. Incidence of subarachnoid hemorrhage: role of region, year, and rate of computed tomography: a meta-analysis. Stroke. 1996;27(4):625–9.
17. Yousem DM, Grossman RI. Neuroradiology: the requisites. 3rd ed. Philadelphia: Mosby; 2010.
18. Manno EM. Subarachnoid hemorrhage. Neurol Clin. 2004;22(2): 347–66.
19. Kassell NF, Torner JC, Haley Jr EC, Jane JA, Adams HP, Kongable GL. The international cooperative study on the timing of aneurysm surgery. Part 1: overall management results. J Neurosurg. 1990;73(1):18–36.
20. Provenzale JM, Hacein-Bey L. CT evaluation of subarachnoid hemorrhage: a practical review for the radiologist interpreting emergency room studies. Emerg Radiol. 2009;16(6):441–51.
21. Wintermark M, Ko NU, Smith WS, Liu S, Higashida RT, Dillon WP. Vasospasm after subarachnoid hemorrhage: utility of perfusion CT and CT angiography on diagnosis and management. AJNR Am J Neuroradiol. 2006;27(1):26–34.
22. Marshall SA, Kathuria S, Nyquist P, Gandhi D. Noninvasive imaging techniques in the diagnosis and management of aneurysmal subarachnoid hemorrhage. Neurosurg Clin N Am. 2010;21(2):305–23.